Oxid Met (2017) 87:757–766
DOI 10.1007/s11085-017-9749-x

ORIGINAL PAPER

Chlorine Attack of Carbon Steel Between 350 and 500 °C and Its Importance Regarding Corrosion in Waste Incineration

Ludmila Krumm[1] · **Mathias C. Galetz**[1]

Received: 2 February 2017 / Published online: 6 March 2017

Abstract Corrosion in waste to energy (WTE) plants is an extremely interesting issue, involving complex atmosphere and deposit interactions. In this work, the influence of the complex WTE atmosphere and its various constituents was simulated between 350 and 500 °C in order to obtain a better understanding of the corrosion mechanisms occurring in such atmospheres. For this purpose, the typical flue gas mixture of WTE plants was reduced to simpler systems, and the impact of gaseous species typically contained in WTE plants atmospheres on the corrosion rate of the carbon steel 16Mo3 was investigated. Four different atmospheres were used in this work: "full" WTE atmosphere 0.1%HCl + 0.01%SO_2 + 8%O_2 + 17H_2O + 10%CO_2 + N_2, 0.1%HCl + 15 ppmO_2 + 0.01%SO_2 + N_2, 0.1%HCl + 15 ppmO_2 + N_2, and 0.1%HCl + 450 ppmO_2 + N_2. All exposures were carried out in the temperature range between 350 and 500 °C (30 °C steps) for up to 900 h. Parabolic, paralinear, and linear mass change dependent on time, temperature, and atmosphere was observed, the metal consumption as a function of temperature was determined, and the corrosion scales were analyzed and compared with results of field tests. Finally it is shown that the test results obtained from low-oxygen atmospheres match best the corrosive scales observed in field-tested samples.

Keywords Chlorine corrosion · Carbon steel · Waste incineration · High temperature

✉ Mathias C. Galetz
galetz@dechema.de; konrad@dechema.de

[1] Dechema-Forschungsinstitut (DFI), Theodor-Heuss-Allee 25, 60486 Frankfurt am Main, Germany

Introduction

Chlorine-induced corrosion observed in WTE boilers has been a subject of research for several decades [1–4, 20]. However, the detailed corrosion mechanisms are still under debate. Typical corrosion scales found on field-tested tubes of carbon steels under salt deposits have been reported to consist of iron chloride $FeCl_2$ at the metal interface, followed by a mixed iron oxide scale of hematite and magnetite. In some cases, also iron sulfide FeS is reported to form between the chloride and the oxide scale [5]. "Active oxidation" has been proposed as a model to describe the corrosion mechanism under WTE deposits [6]. This model is based on a cyclic process. Chlorine from the environment diffuses inwards through pores and cracks of the oxide scale to the substrate/scale interface and forms metal chlorides due to low oxygen partial pressures beneath the scale. Subsequently, volatile chlorides are formed, which diffuse outwards. On their way out, the metal chlorides are oxidized to Fe_2O_3 due to an increasing oxygen partial pressure near the scale/gas interface. The chlorine is released according to Eq. (1) migrating either to the gas or back to the metal surface for further attack.

$$2FeCl_2 + \frac{3}{2}O_2 = Fe_2O_3 + 2Cl_2 \quad (1)$$

Several authors such as Kautz and Tichatschke [7] or Pasten [8] report that carbon steels in HCl-containing oxygen-rich atmospheres do not produce chlorides in the corrosion scales when exposed in the temperature range of 400 °C. Additionally the corrosion rate was reported unexpectedly low. Ihara et al. [9] found that the ratio of oxygen to hydrogen chloride in the process gas mixture also has a significant influence on the corrosion rate at high temperatures. At 400 °C, the maximum corrosion rate is reported at an oxygen/hydrogen chloride ratio of 65–35% (O_2:HCl = 1:0.5), while at higher temperature (500–600 °C) the maximum shifts-to-lower oxygen ratios of 20% (O_2:HCl = 1:4). Unfortunately there is no information about the corrosion scales in [9]. In this work, the impact of atmospheres with different oxygen content on both the corrosion rate and the nature of corrosion products will be investigated.

Experimental Procedures

The material 16Mo3 (1.5415) was delivered by a commercial supplier as rods with a diameter of $d = 8$ mm. The chemical composition of the material is given in Table 1. The rods were ground with 400-grit SiC paper in order to ensure an oxide-free sample surface and then cut into cylindrical pieces with a length of $l = 15$ mm.

Table 1 Chemical composition of 16Mo3 (1.5415)

Element	C	Ni	Mn	Cr	Mo	Si	Al
(%)	0.12–0.2	≤0.3	0.4–0.9	≤0.3	0.25–0.35	≤0.35	≤0.04

After cleaning the samples in ethanol, they were measured and placed in alumina crucibles. Several weighing steps were conducted after exposure: net specimen, specimen with alumina crucible, and specimen plus debris found in the crucible. Hence, also spalled and sublimated corrosion products on crucible walls can be distinguished.

All samples were exposed in a six-zone furnace within two separate quartz tubes under constant gas flow of 3 l/h. This way it was possible to use two different atmospheres and six different exposure temperatures at a time. The testing temperatures were between 350 and 500 °C in 30 °C steps with exposure times of 300, 600, and 900 h. It is important to note that the 600-h exposure was stopped once, when the 300-h samples were removed. This one additional cycle can explain certain deviations from the data observed after 300 and 900 h. The 300 and 900 h tests were not interrupted. Pretests were conducted to ensure that flowing the gas first through the low-temperature zone and then through zones with rising temperatures or the other way around did not influence the outcome. The oxygen partial pressure of the different atmospheres was measured using an oxygen analyzer (Rapidox 2000 Cambridge Sensotec). The composition of the atmospheres used is listed in Table 2. The oxygen amount of 15 ppm was the lowest achievable due to gas impurities. The composition taken as "full" WTE atmosphere was chosen in accordance with flue gas composition during waste incineration [10]. An additional exposure was carried out in synthetic air at 440 °C as reference. All samples were heated up in dry N_2 atmosphere, after reaching the desired temperature the quartz tube was fed with process gas.

The mass change of the samples was determined by weighing two samples each before and after exposure. After the mass change was determined, the corrosion products were removed and the samples were weighed again in order to quantify the material wastage. The product removal was carried out with an inhibitor containing HCl solution, as described in detail [19]. During the cleaning procedure, the samples were weighed several times. The cleaning procedure was carried out until the change of the mass reached the corrosion rate of 0.2 mg/cm^2 h of untreated samples, but no longer than 2 h. This product removal ensures that the sample substrate is not attacked significantly.

Table 2 Exposure conditions

No.	Exposure time (h)	Exposure temperature (°C)	Atmosphere (%)
1	300, 600, 900	350–500 in 30 °C steps	0.1%HCl + 0.01%SO_2 + 8%O_2 + 10%CO_2 + 17%H_2O (full WTE plant atmosphere)
2	100, 300	350–500 in 30 °C steps	0.1%HC + 8%O2 + 10%CO2 + 17%H_2O
3	300, 900	440	Synthetic air
4	300, 600, 900	350–500 in 30 °C steps	0.1%HCl + 15 ppm O_2 + 0.01%SO_2 + rest N_2
5	300, 600, 900	350–500 in 30 °C steps	0.1%HCl + 15 ppm O_2 + rest N_2
6	100, 300	350–500 in 30 °C steps	0.1%HCl + 450 ppm O_2 + rest N_2

Furthermore, the microstructure and morphology of the corrosion product were investigated by using LOM and microprobe (EPMA). All cross sections were prepared water-free as described in [11].

Results and Discussion

Oxygen-Rich Simulated WTE Plant Atmospheres

(0.1%HCl + 0.01%SO_2 + 8%O_2 + 10%CO_2 + 17%H_2O) With and Without 0.01% SO_2 Addition in Comparison with Synthetic Air

After the corrosion tests in simulated WTE plant atmosphere, all samples show corrosion scales similar to those known from air exposure [12], with no chlorides or sulfides in the scale. The scale consists of iron oxides and shows an oxygen gradient toward the substrate surface. Microprobe results show a composition in accordance with outer hematite and inner magnetite. To demonstrate this similarity, an additional sample was exposed in air for 900 h at 440 °C. In Fig. 1, the elemental maps of this sample are compared to one exposed in the "full" simulated WTE plant atmosphere exposed for 900 h at 440 °C. This figure confirms the similarity. However, it should be mentioned that, although the scale looks similar, the metal wastage after 300 h was higher in the "full" WTE atmosphere 1 than with air exposure at 440 °C. Even though no chlorides were found in the scale, the increase in material wastage compared to synthetic air proves the effect of chlorine and sulfur. Pasten et al. [5] found comparable values for material wastage at similar conditions. The chlorine-containing molecules in the simulated plant atmosphere seem able to accelerate the attack on the substrate surface, but, due to the comparatively high oxygen partial pressure in the gas mixture, oxidation dominates the formation of corrosion products in the scale.

As expected, mass change and material degradation of samples exposed to simulated WTE plant atmospheres increase with exposure time and temperature.

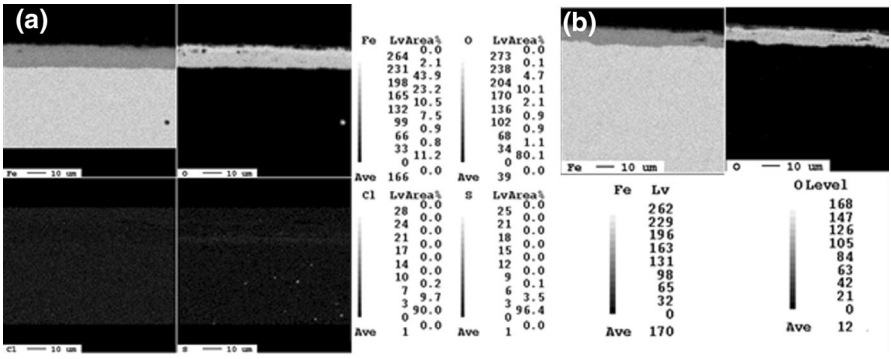

Fig. 1 Elemental map of 16Mo3 **a** after 900 h at 440 °C in simulated WTE plant atm. no. 1 **b** after 900 h at 440 °C in synthetic air (atm. no. 3)

The data points after 600 h exposure at 500 °C were neglected in the discussion, as they show a huge error due to scale cracking during the interruption after 300 h. Anyway, the standard deviation shows that all the other data points are reliable and representative for the results at atmospheres with high oxygen partial pressure. It can be observed that the increase during exposure time for material degradation as well as for mass gain becomes smaller. The fit by a parabolic function confirms the observation. Furthermore, from the parabolic fit the parabolic rate constants k_p have been determined and are shown in Fig. 2b. These k_p values at different temperatures are comparable to those listed in [12] for iron oxidation at low temperatures in air. Thus, it can be concluded that protective oxide scales are formed predominantly. Evaporation processes due to volatile chloride formation can be neglected in atmospheres with high oxygen partial pressure.

In Fig. 3, the difference between atmospheres 1 and 2 and the influence of SO_2 (or rather SO_3 at this temperature) on mass change as function of temperature are presented. The atmosphere without SO_2 causes lower mass increase as well as a lower material wastage above 380 °C than the simulated plant atmosphere containing SO_2. Furthermore, corrosion scales in atmosphere no. 2 do not exhibit the typical iron oxide scales of magnetite and hematite, only oxygen-rich scales with the iron-to-oxygen ratio of 2:3 are found.

Low-Oxygen Content Atmospheres

Results for the Atmospheres: 0.1% (1056 ppm) HCl + 15 ppm O_2 + rest N_2 and 0.1% (1056 ppm)HCl + 15 ppm O_2 + 0.01%SO_2 + rest N_2

When the oxygen partial pressure is strongly decreased from 8 vol% to a measured partial pressure of only 15 ppm, the impact of SO_2 is much stronger. Material degradation in SO_2-containing atmosphere (atm. no. 4) shows four times higher values compared to the atmosphere without SO_2 (atm. no. 5) as shown in Fig. 4.

Both atmospheres 0.1% (1056 ppm) HCl + 15 ppm O_2 + rest N_2 and 0.1% HCl + 15 ppm O_2 + 0.01%SO_2 + rest N_2 led to comparable results, in which,

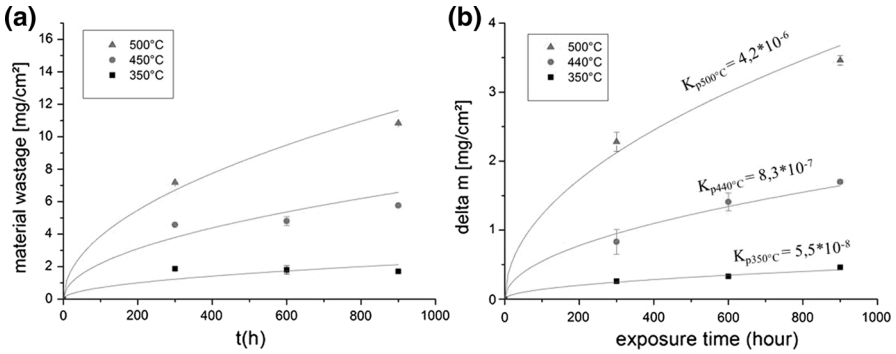

Fig. 2 **a** Material wastage of 16Mo3 as function of exposure time at selected temperatures. **b** Mass change (delta m) as function of exposure time and temperature in atm. no. 1 with parabolic rate constant k_p (mg^2/cm^4s) received from parabolic fit

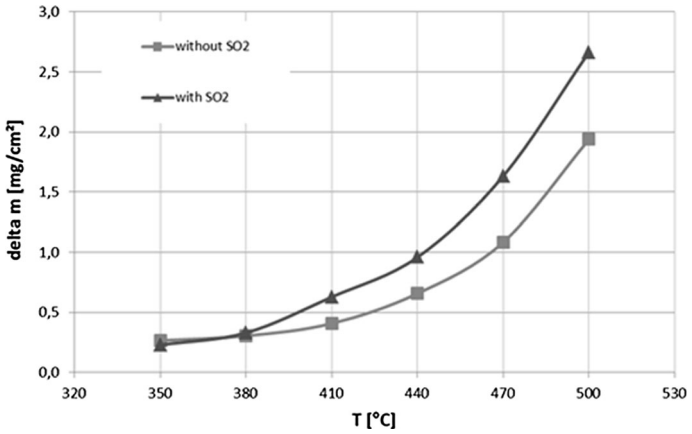

Fig. 3 Mass change over time in atmospheres 1 (0.1%HCl + 0.01%SO2 + 8%O2 + 10%CO2 + 17%H_2O) and 2 (0.1%HCl + 8%O2 + 10%CO2 + 17%H_2O)

depending on exposure temperature, three different typical mass change curves can be distinguished: parabolic, paralinear, and linear types. At low temperatures up to 410 °C, a parabolic mass change behavior as a function of time occurred. Above 410 °C, the linear kinetics rate becomes more and more obvious, until it dominates at 500 °C as shown in Fig. 5. For the mass change calculation, only the spalled corrosion products and the corrosion products adherent to the sample were considered, but not those that were found on the crucible walls, where a thick layer of iron oxide was deposited in the temperature range of 440–500 °C.

If such corrosion products were added to the mass change, a linear increase in mass would result, which is not shown to avoid misleading conclusions. Instead of a strong evaporation, a linear scale growth could be concluded. This demonstrates the importance of looking at the metal wastage and scale morphologies when volatile corrosion products are involved in the corrosion mechanism in addition to mass gain curves.

Appearance of such typical different kinetics in chlorine-containing atmosphere was already observed in previous publications, e.g., Foroulis [13]. Paralinear

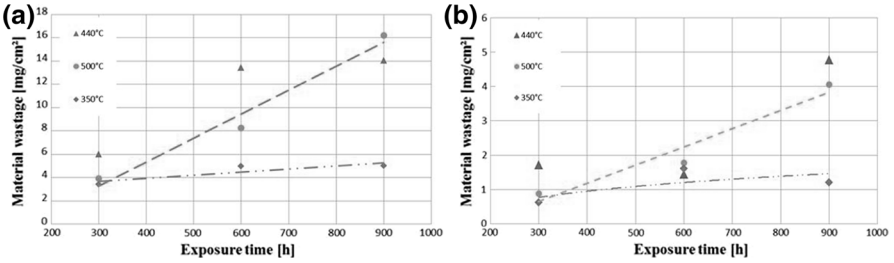

Fig. 4 Material wastage as function of time for different exposure temperatures in the atmospheres **a** 0.1%HCl + 0.01%SO_2 + 15 ppm O_2 + rest N_2 and **b** 0.1%HCl + 15 ppm O_2 + rest N_2

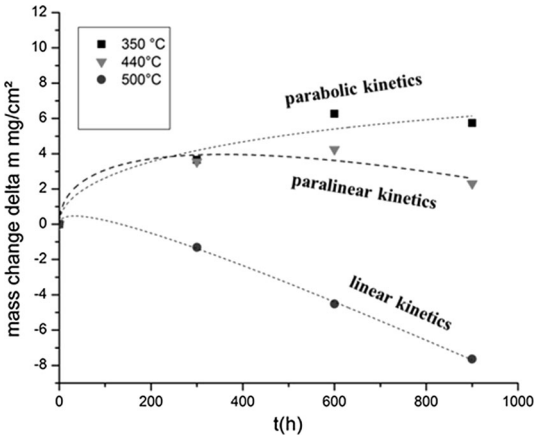

Fig. 5 Mass change as function of exposure time for different exposure temperatures in 0,1%HCl + 0,01%SO_2 + 15 ppmO_2 + Rest N_2 atmosphere

kinetics behavior is caused by a parabolic rate of weight gain and a linear weight loss which proceed simultaneously. Comparison with literature [14] shows that at temperatures below $T < 400$ °C in HCl-containing atmospheres mainly solid scale formation determines the corrosion rate. In accordance with the present work, at temperatures above 400 °C vaporization of iron chlorides becomes more important for the reaction rate. In order to quantify the chlorination kinetics, the experimental data were fitted by Eq. 2, whose applicability to high temperature involving volatile corrosion was discussed in detail in [15]:

$$x = k_p t^{0.5} - k_v t \tag{2}$$

where x is the mass change per unit area at time t, k_p is the parabolic rate constant for scale growth, and k_v is the linear weight loss rate by volatilization. The fitting parameters are summarized in Table 3 and approve the transition in the mechanism.

At 350 °C, as expected, the linear weight loss rate is negligible in comparison with higher temperature, and scale formation on the substrate surface determines the material degradation. The situation is different in the case of the 500 °C exposure, where the linear weight loss parameter defines the corrosion mechanisms and the parabolic rate is negligible. Interestingly, at 440 °C the resulting k_p is about double the value of the one at 350 °C and six times higher than at 500 °C, while the evaporation rate already almost matches that at 500 °C. These high fitting parameters suggest the highest material degradation at intermediate temperatures, which was confirmed by the results of material wastage at the different temperatures. Figure 4 shows an increase in material wastage with increasing temperature up to 440 °C and a decrease at higher temperatures. This observation of a maximum in the metal consumption within the range of transition from dominant parabolic to linear behavior was also published by Tseitlin and Strunkin [16].

Table 3 Parabolic rate constant and weight loss parameter extracted from fit of Eq. (2)

Temperature (°C)	k_p (mg^2/cm^4 h)	k_v (mg/cm^2 h)
350	0.085	0.003
440	0.176	0.011
500	0.03	0.014

Results for the Atmosphere 0.1% (1056 ppm) HCl + 450 ppm O_2 + rest N_2

Since the reduction of the oxygen partial pressure has such a huge effect on the corrosion behavior, a third oxygen partial pressure was tested (atm. no. 6). Detailed investigation of the scales shows that the scale thickness remains nearly constant with further exposure time at 350 °C while it continues its growth at an exposure temperature of 440 °C. The corrosion layer consists of two layers with a scale thickness of already 40–50 µm after 100 h exposure time. The inner scale consists of a mixture of iron, chlorine, and oxygen, while the outer scale consists of iron oxide (see Fig. 6). In comparison with tests carried out in atmospheres with high oxygen content, the material degradation in 0.1%HCl + 450 ppmO_2 + rest N_2 increased by a factor of 5 at temperatures of 440 °C and by a factor of 8 in atm. no. 5 at the same temperature. The most interesting observation made in this atmosphere is the presence of prominent iron oxide crystals within the scale (a). Their presence is attributed to the occurrence of chlorides that are well known to directly produce hematite when transformed into oxides [17]. However, in our case, the octahedral shape of the crystals in combination with the Fe/O ratio suggests the crystals to be maghemite (γ-Fe_2O_3). Interestingly, such hematite crystals also formed at the alumina crucible walls (Fig. 7b). The formation of those Fe_2O_3 crystals far away from the sample surface is only possible with enhanced iron chloride evaporation and active oxidation. This is also a valuable hint of the influence of the oxygen partial pressure in the corrosion process because the volatile chlorides must react with oxygen to nucleate the oxide crystals. On the surface of

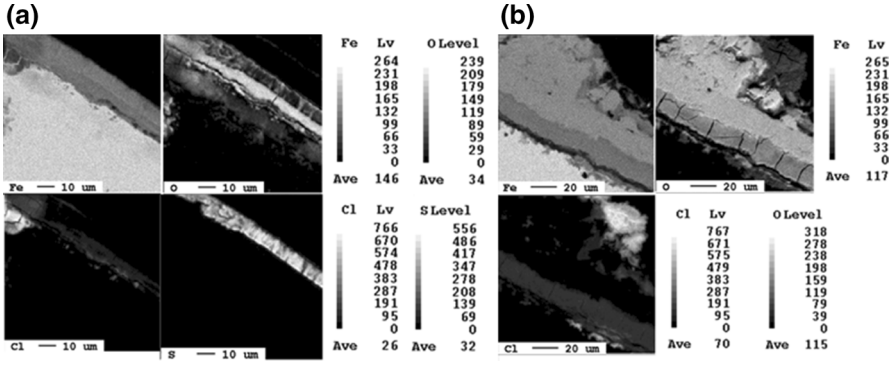

Fig. 6 Elemental map of 16Mo3 after 300 h at 440 °C in **a** 0.1%HCl + 0.01%SO_2 + 15 ppm O_2 + rest N_2 and **b** 0.1%HCl + 450 ppmO_2 + rest N_2

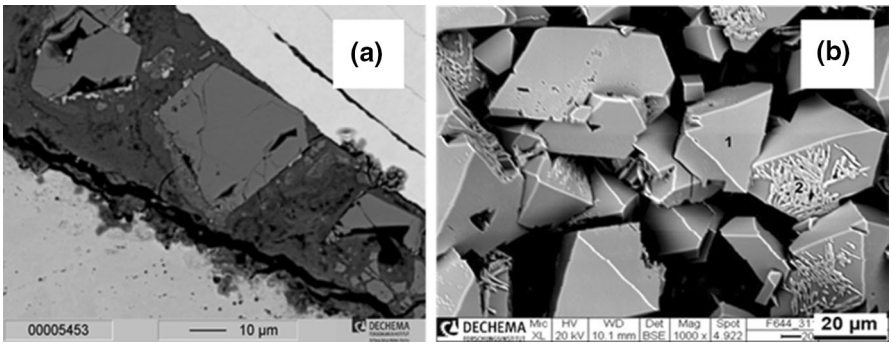

Fig. 7 **a** Iron oxide crystal formation on sample surface after exposure at 440 °C in 0.1%HCl + 450 ppmO_2 + rest N_2 atmosphere and **b** iron oxide single crystals, found on crucible wall at 500 °C in atm. no. 4

some of those crystals, FeS was detected (spot 2 in Fig. 7b), while other only show Fe_2O_3 (e.g., at spot 1 in Fig. 7b). This indicates that SO_2/SO_3 can oxidize iron chlorides as well. Finally, the crystals grow in the thermodynamically most stable iron oxide form. If oxygen is abundant, this oxidation of the chlorides is suggested to occur instantly at the sample surface. At 500 °C after 100 h testing, the corrosion scale consists of an only few µm thick iron oxide scale with some chlorine traces, and the volatile chlorides are transported with the gas stream from the sample and crucible surface. In accordance with the results of Ihara [9], who suggested the high impact of the oxygen-to-chlorine ratio, the corrosion rate of the present gas mixture lies within the region of high corrosion rates. SO_2 also seems to have a huge impact on the chloride to oxide transformation, since the atmospheres 0.1%HCl + 0.01%SO_2 + 15 ppm O_2 + rest N_2 and 0.1%HCl + 450 ppmO_2 + rest N_2 at 440 °C cause the highest metal consumption of all conditions investigated in this work. As the usual operating temperatures of superheater tubes are between 420 and 450 °C, a clarification of the corrosion mechanisms especially at such intermediate temperatures is of huge interest and has to be investigated in more detail in further work. It is also remarkable that the scale after testing in the atmosphere 0.1%HCl + 0.01%SO_2 + 15 ppm O_2 + N_2 at 440 °C shows a similar structure and scale composition as reported for corrosion scales on field-tested tubes—exposed to the "full" WTE atmosphere but with additional deposits.

Conclusions

In accordance with [9], the results of this study show that the oxygen-to-chlorine ratio has a huge influence not only on the corrosion rate but also on the corrosion products. A "full" simulated WTE atmosphere with 8 vol% oxygen does not lead to the typical corrosion scales found on field-tested tubes. Instead the scale formation and morphology is rather similar to synthetic air exposures. It can be concluded that in chlorine-containing atmospheres with high oxygen content the chlorine influence can be neglected, since chlorides that might form are directly transformed into

oxides and thereby contribute to the scale formation. This mechanism might be similar to the one described for halogen-enhanced alumina formation at much higher temperatures [18]. However, the highest values of metal consumption among the various tests and temperatures in this work were found at 440 °C in oxygen-reduced atmospheres ($0.1\%HCl + 0.01\%SO_2 + 15$ ppm $O_2 +$ rest N_2 and $0.1\%HCl + 450$ ppm$O_2 +$ rest N_2). Reaction kinetics considerations have shown that the most critical case occurs when both the parabolic and the linear rate constants are significant and high. Interestingly, in $0.1\%HCl + 0.01\%SO_2 + 15$ ppm $O_2 +$ rest N_2 atmosphere, corrosion scales similar to those found on field-tested superheater tubes in WTE plants are formed, where the gas contains about 8 vol% oxygen, but deposits build up on the superheater tubes. It has to be investigated how the deposits might change the atmosphere in a way that ultimately forms corrosion scales equal to those found in this work at low oxygen partial pressures.

Acknowledgements The Federal Ministry of Education and Research (BMBF) is gratefully acknowledged by the authors for supporting this work within the frame of "MatRessource." Additionally the authors thank Mathias Röhrig for technical support and Gerald Schmidt for the EPMA analysis.

References

1. D. P. Miller, H. H. Krause, A. D. Vaughan and K. W. Boyd, *Corrosion* **28**, 1972 (274).
2. H. J. Grabke, in *Incinerating Municipal and Industrial Wastes*, ed. R. W. Bryers, Hemisphere, (New York, 1990), p. 161.
3. R. Bender and M. Schütze, in *Solutions of corrosion Problems in advanced Technologies: Proceedings of Eurocorr 1999, Aachen*, ed. G. Schmitt, M. Schütze, (1999).
4. M. Spiegel, *Materials and Corrosion* **50**, 1999 (373).
5. H. H. Krause, *Materials for Energy Systems* **7**, 1986 (322).
6. H. J. Grabke, E. Reese and M. Spiegel, *Corrosion Science* **37**, 1995 (1023).
7. K. Kautz and J. Tichatschke, *VGB Kraftwerkstechnik* **52**, 1972 (249).
8. M. S. Pasten, "Korrosionsverhalten von Eisen, einem niedriglegierten Stahl, 9% Cr Stählen, Nickel und einem Ni-Basislegierung unter einer simulierten Müllverbrennungsatmosphäre und Chlorid-Sulfat-Ablagerungen bei erhöhter Temperatur.", Ph.D. Thesis, Universtität Dortmund (2006).
9. Y. Ihara, H. Ohgame, K. Sakiyama and K. Hashimoto, *Corrosion Science* **21**, 1981 (805).
10. www.prewin.eu – European Network: Performance, Reliability and Emissions Reduction in Waste Incinerators.
11. K. Rahts, M. Schorr, C. Schwalm and M. Schütze, *Praktische Metallographie* **36**, 1999 (86).
12. N. Bertrand, C. Desgranges, D. Poquillon, M. C. Lafont and D. Monceau, *Oxidation of Metals* **73**, 2010 (139).
13. Z. A. Foroulis, *Anti-corrosion Methods and Materials* **35**, 1988 (4).
14. R. J. Fruehan and L. J. Martonik, *Metallurgical Transactions* **4**, 1973 (2789).
15. A. Soleimani-Dorcheh, W. Donner and M. C. Galetz, *Materials and Corrosion* **65**, 2014 (1143).
16. K. L. Tseitlin and V. A. Strunkin, *Journal of Applied Chemistry of the USSR* **31**, 1958 (1832).
17. A. W. Henderson, T. T. Campbell and F. E. Block, *Metallurgical Transactions* **3**, 1972 (2579).
18. M. Schütze and M. Hald, *Materials Science and Engineering A* **239–240**, 1997 (847).
19. *NACE International Standard Recommended Practice—Preparation, Installation, Analysis, and Interpretation of Corrosion Coupons in Oilfield Oparations* (2005).
20. M. J. McNallan, W. W. Liang, S. H. Kim and C. T. Kang, in *Proceedings of High Temperature Corrosion, San Diego California*, 2–6 March 1981, ed. R. A. Rapp, (NACE, 1981), p. 316.